Frontiers in Dentistry

# Tissue Response and Osteoconductive Properties of Forsterite/Poly Lactic Acid Hybrid Nano-Composite Scaffold in Rat

Parichehr Behfarnia[1]*, Paria Biglary[2], Mohammad Tavakoli[1], Seyed Mohammad Razavi[3], Seyed Amir Mirghaderi[4], Saman Naghieh[5], Ehsan Foroozmehr[6], Mahshid Kharaziha[7]

1. Department of Periodontics, Dental Implants Research Center, Dental Research Institute, School of Dentistry, Isfahan University of Medical Sciences, Isfahan, Iran
2. Department of Periodontics, School of Dentistry, Ardebil University of Medical Sciences, Ardebil, Iran
3. Department of Oral and Maxillofacial Pathology, Torabinejad Dental Research Center, School of Dentistry, Isfahan University of Medical Sciences, Isfahan, Iran
4. Dental Biomaterials Department, School of Dentistry, Tehran University of Medical Sciences, Tehran, Iran.
5. Division of Biomedical Engineering, Collage of Engineering, University of Saskatchewan, Saskatoon, SK, Canada
6. Department of Mechanical Engineering, Isfahan University of Technology, Isfahan, Iran
7. Department of Material Engineering, Isfahan University of Technology, Isfahan, Iran

**Article Info**

***Article type:***
Original Article

***Article History:***
Received: 28 Jun 2024
Accepted: 18 Jan 2025
Published: 24 Jul 2025

**** Corresponding author:***
Department of Periodontics, School of Dentistry, Isfahan University of Medical Sciences, Isfahan, Iran

Email: dr.pbehfarnia@gmail.com

**A B S T R A C T**

**Objectives:** Objectives: The present research aimed to evaluate the potential of three-dimensional (3D) poly lactic acid (PLA) microstrut scaffolds, surface-modified with nanocomposite gelatin-forsterite fibrous layers possessing porosities of 40% and 70%, to facilitate bone regeneration and angiogenesis in a rat model.

**Materials and Methods:** Thirty-six rats, each with a surgically created cranial defect measuring 4 mm in radius, were randomly assigned in a 1:1:1 ratio to one of three experimental groups: A 40% scaffold group (G1), a 70% scaffold group (G2), and a control group receiving no scaffold (G3). Animals were euthanized at either 4 or 8 weeks post-surgery. Histological analysis using hematoxylin and eosin (H&E) staining was performed to observe the tissue response and bone formation within the surgical defects. Histomorphometric assessment was employed to quantify the percentage of newly formed woven and lamellar bone in each group.

**Results:** The mean percentages of total bone formation at 4 weeks were 33.55±4.32%, 37.76±6.20%, and 33.66±2.30% in groups G1, G2, and G3, respectively. At 8 weeks, the corresponding mean percentages were 34.25±1.94%, 37.33±4.30%, and 35.16±3.68% for the same groups. Statical analysis revealed a significant difference in angiogenesis between G1 and G2 at 8 weeks ($p \leq 0.01$).

**Conclusion:** Our findings demonstrated that the fabricated scaffold exhibited the capacity to facilitate osseous tissue development and promote osteoblast adhesion and infiltration. The scaffolds with 70% porosity showed superior performance in total bone formation compared to those with 40% porosity. This novel scaffold design holds promise for enhancing both angiogenesis and osteogenesis processes.

**Keywords:** Tissue Scaffolds; Printing; Three-Dimensional; Poly (Lactic Acid); Forsterite; Osteogenesis

➢ **Cite this article as:** Behfarnia P, Biglary P, Tavakoli M, Razavi SM, Mirghaderi SA, Naghieh S, et al. Tissue Response and Osteoconductive Properties of Forsterite/Poly Lactic Acid Hybrid Nano-Composite Scaffold in Rat. *Front Dent.* 2025:22:29. http://doi.org/10.18502/fid.v22i29.19213

## INTRODUCTION

Reconstruction of bone defects presents a significant challenge in both periodontal therapy and implant dentistry [1-5]. Enhancing bone regeneration can be achieved through the implementation of biocompatible and resorbable scaffolds. These scaffolds facilitate the migration of osteogenic cells from adjacent viable bone tissue and promote the deposition of new bone within their structure [6]. To enhance bone regeneration, porous scaffolds have been fabricated using a variety of natural and synthetic polymers, as well as ceramics, each presenting unique advantages and limitations. Given that natural bone is a composite of organic and inorganic constituents, polymer/ceramic combinations have garnered significant interest within this domain [7]. Porous scaffolds facilitate tissue regeneration and angiogenesis, a process crucial for supplying nutrients and oxygen to developing tissues. For instance, the vascularization of tissue constructs exceeding a critical size of approximately 100-200 mm necessitates the formation of new blood vessels. Pore dimensions and the interconnectedness of macro-pores represent key determinants in promoting angiogenesis; consequently, scaffolds lacking porosity exhibit limited bioactivity in tissue engineering applications [8].

Polymeric scaffolds necessitate an optimal porosity level, ideally around 90%, while concurrently maintaining maximal mechanical properties to facilitate adequate cellular infiltration and provide a sufficient surface area for effective cell-polymer interactions [9]. Conversely, the reconstruction of orthopedic defects necessitates the utilization of poly (lactic-co-glycolic acid) (PLGA) scaffolds exhibiting a porosity level below 80%. Porosity exceeding this threshold may compromise the structural integrity of the scaffold [10]. It is important to note that the optimal porosity is contingent upon a multitude of factors, including the specific orthopedic application, the requisite mechanical load-bearing capacity, and the desired rate of scaffold degradation. Scaffolds exhibiting medium-sized macro-pores demonstrate a more rapid degradation rate compared to those with smaller pore dimensions. This accelerated resorption is correlated with a histological profile characterized by a reduced presence of bone tissue and a higher proportion of connective tissue; however, this compositional disparity diminishes over time [11].

Scaffolds intended for bone regeneration applications must exhibit a balanced profile encompassing mechanical properties, in vivo degradation kinetics, and diffusion capabilities [9]. Furthermore, the dimensions of the fabricated scaffolds should precisely correspond to the spatial extent of the bone defect. Biodegradable synthetic polymers, such as poly (lactic acid) (PLA) and PLGA, are frequently employed in tissue engineering contexts owing to their inherent biocompatibility [12]. PLA, a resorbable polyester, finds widespread application in drug delivery systems and tissue regeneration owing to its favorable mechanical properties, controllable degradation kinetics, and exceptional biocompatibility [13]. Nanostructured forsterite ($Mg_2SiO_4$), a bioceramic material, exhibits optimal biocompatibility and, in contrast to its microstructural counterpart, possesses bioactive properties. Forsterite exhibits superior mechanical properties (hardness and fracture toughness) compared to calcium-phosphate ceramics, glass, and glass-ceramics. Nevertheless, scholarly investigations concerning the synthesis and characterization of composite materials comprising polymers and forsterite are currently limited in scope [7].

The present research aimed to evaluate and contrast the tissue response and osteogenic potential elicited by a forsterite/PLA hybrid nanocomposite scaffold fabricated with two distinct porosity levels.

## MATERIALS AND METHODS

This study adhered to the ethical principles outlined in the Declaration of Helsinki and received approval from the Ethics Committee of Isfahan University of Medical Sciences (reference number: IR.MUI.REC.1394.3.1017).

***Materials:***

This investigation utilized gelatin (Type-A, derived from bovine skin), acetic acid, and N,N-(3-dimethylaminopropyl)-N'-ethyl-carbodiimide hydrochloride (EDC), all sourced from Sigma (Germany). Synthesized Forsterite nanopowder (sol-gel method) utilizing magnesium nitrate hexahydrate ($Mg(NO_3)_2 \cdot 6H_2O$, Merck, 99.99% purity), was incorporated into the study. PLA (translucent and clear) was procured from Bits from Bytes Ltd. (Clevedon, UK) in the form of 2.7mm diameter filaments.

***Preparation of Rats:***

This research utilized 36 male Wistar rats, approximately six months of age and weighing between 270 and 350g. All experimental procedures adhered to the ethical guidelines for animal research, as approved by the Institutional Animal Care and Use Committee at Isfahan University of Medical Sciences. The animals were housed in a climate-controlled room under a 12-hour light/dark cycle at a consistent temperature of 22±2°C, with access to both water and standard rat chow. Following veterinary confirmation of systemic health, the rats were enrolled in the study then maintained in individual cages for a one-week acclimatization period prior to any experimental procedures. No premedication was administered to the animals.

Rats were randomly assigned to one of three experimental groups in a 1:1:1 ratio: Group 1 (G1), receiving a 40% scaffold; Group 2 (G2), receiving a 70% scaffold; and a control group (G3) receiving no scaffold.

***Preparation of Scaffolds:***

The detailed methodology for fabricating forsterite/PLA hybrid nanocomposite scaffold utilizing fused deposition modeling (FDM) and electrospinning techniques has been comprehensively documented in previous publications [14, 15]. In brief, the FDM technique was employed for the creation of PLA scaffolds. Two distinct G-code file sets were developed for the RAPMAN 3.2 FDM apparatus (Clevedon, UK) to produce scaffolds exhibiting porosities of 40% and 70%. The fabrication parameters included a layer thickness of 0.5mm and a 0-90 lay-down pattern. The interlayer spacing in the G-code was set at 1.69mm for the 70% porosity scaffolds and 1mm for the 40% porosity scaffolds. Fabricated scaffolds (8mm in diameter and 1.5mm in thickness) underwent a coating process involving nanocomposite fibrous gelatin-forsterite layers. This coating was achieved via the electrospinning technique, involving two PLA layers followed by the electrospinning of the gelatin-forsterite nanocomposite on top. The electrospinning solution was formulated by dispersing 10% (w/v) forsterite within a 10% (w/v) gelatin solution, utilizing an 80% (v/v) acetic acid mixture as the solvent. Subsequent to a 1-hour sonication period of the formulated mixture, a 1mL standard syringe (a 23G blunted stainless steel needle) was employed to coat the specimens (a flow rate of 1mL/h, a collector-to-needle distance of 18cm, and an applied voltage of 17kV). To induce crosslinking of the gelatin component post-electrospinning, the scaffolds were immersed in a 75mM EDC solution in 90% (v/v) ethanol for 12 hours at 4°C. Following the crosslinking reaction, the scaffolds underwent a washing procedure using phosphate-buffered saline (PBS). Furthermore, the particle size of the forsterite material was determined through the analysis of transmission electron microscopy (TEM) micrographs, acquired using a Zeiss EM900 instrument. This analysis, performed with ImageJ software, revealed a particle size range of 25 to 45nm.

***Surgical Procedure:***

General anesthesia was initiated through the inhalation of halothane. Following the preparation of the surgical site via shaving and disinfection with a 10% povidone-iodine solution, a one-centimeter incision was made in the scalp. Subsequent to the retraction of the skin and the underlying periosteum, a standardized bone defect, measuring 8 mm in diameter and 1.5mm in depth, was created in the parietal bone of the calvaria along the mid-sagittal suture using a trephine bur (Meisinger, Germany). With the exception of the control group, one randomly selected scaffold was implanted into each of the created bone defects (Figure 1).

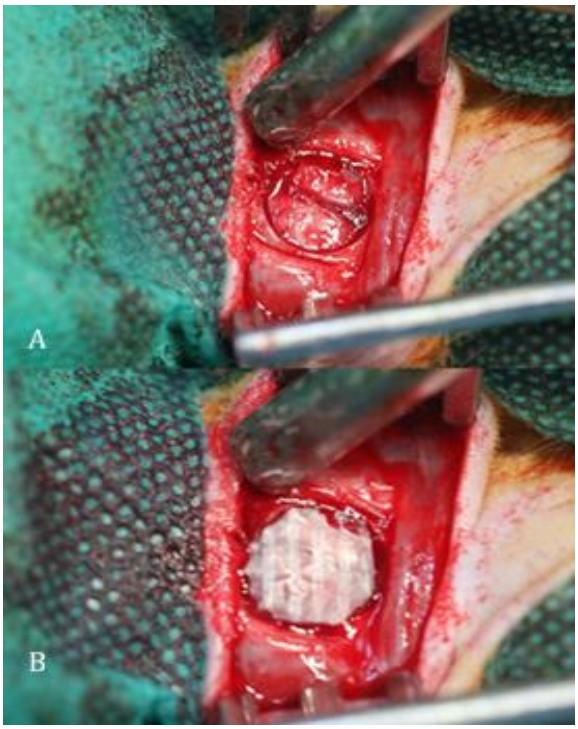


**Fig 1.** A) Bone defect created at the mid-sagittal suture of the calvarias. B) Scaffold placed in bone defect

Following the surgical procedure, the flap was repositioned, and the periosteum was closed with absorbable polyglycolic acid sutures (19, 4-0, polyglycolic coated violet, Supa Medical Devices, Iran). and the skin was closed using non-absorbable silk sutures (19, 4-0, braided black silk, Supa Medical Devices, Iran). Post-operatively, flunixin meglumine analgesic (2.5mg/kg; Razak Laboratories, from active material supplied by Norbrook, Ireland) and cefazolin antibiotic (15mg/kg; Dana Pharmaceutical Company, Tabriz, Iran) were administered immediately and then once daily for three consecutive days. The sutures were removed between 10 and 14 days post-surgery. Following the surgical intervention, the rats were individually housed in separate cages and subsequently identified using a coding system. The date on which each surgery was performed, along with the assigned experimental group for each rat, was also documented. A veterinary professional conducted regular examinations of the animals. In total, 36 distinct defects were generated throughout the study, with each experimental group comprising 12 defects. Within each group, six rats were euthanized at the four-week postoperative time point, and the remaining six were euthanized at the eight-week postoperative time point. Consequently, six defects within each group were available for analysis at each designated time interval.

***Preparation of Specimens and Histological and Histomorphometric Assessments:***

Following the designated experimental endpoints of 4 and 8 weeks, the animals were euthanized. The calvarial specimens were fixed through immersion in a 10% formalin solution. Decalcification was then performed via immersion in an ethylenediaminetetraacetic acid solution adjusted to a pH of 7.2 and maintained at 37°C for two weeks. Post-decalcification, the samples were stored overnight at 4°C in a PBS solution with a pH of 7.4, supplemented with 6.8% sucrose. Finally, the samples underwent a 60–90-minute incubation period in 100% acetone at 4°C. Afterward, the specimens underwent embedding in hydroxyethyl methacrylate. Serial sections with a thickness of 4µm were prepared using a microtome (Acutumm 50, Struers, Copenhagen, Denmark) and subsequently stained with hematoxylin and eosin (H&E according to Gill's protocol) to evaluate the tissue response and the extent of bone formation. A blinded pathologist conducted a meticulous assessment of the specimens under a light microscope (Nikon YS, Tokyo, Japan) at ×100 magnification to determine the tissue response and the degree of angiogenesis. In histomorphometry evaluation, the proportion of newly formed woven and lamellar bone within the bone defects was quantified. Following histological slide preparation, photomicrographs of the specimens were captured utilizing the digital imaging system of a light microscope (Nikon DP-R Camera, Tokyo, Japan) at magnifications of ×40 and ×100. For each specimen, three digital images were captured (superior, middle, and inferior borders), coded, and saved on a computer. Quantitative analysis of osteogenesis, distinguishing between woven and lamellar bone formation, was performed on each

image utilizing the image analysis capabilities of Adobe Photoshop. The resulting measurements were then recorded as mean values for each specimen. Furthermore, the inflammation severity was specified based on the infiltration level of macrophages, plasma cells, neutrophils, and fibroblasts, assessed as follows:

***Absence of inflammation:*** The absence of inflammatory cells, a fibroblast count>30, and the presence of mature fibrotic tissue exhibiting a high collagen content.

***Slight inflammation:*** The presence of macrophages and plasma cells, with the number of inflammatory cells<30, a fibroblast count between 10 and 30, and the tissue presenting as immature fibrotic tissue with a limited amount of collagen.

***Moderate inflammation:*** The presence of macrophages and plasma cells, focal accumulations of neutrophils, granulocytes, or lymphocytes, number of inflammatory cells between 30 and 60, and a fibroblast count between 5 and 9.

***Severe inflammation:*** Localized areas of necrosis and a significant infiltration of inflammatory cells, the inflammatory cell count>60, and the fibroblast count ranging from 1 to 4 [16-18].

The quantification of newly formed lamellar and woven bone, along with the total volume of new bone tissue, was performed by calculating their respective percentages. The assessment of vascularization was conducted based on the enumeration of blood vessels identified in histological sections stained with H&E [19].

To statistically analyze the data, a two-way analysis of variance (ANOVA) was employed to compare the 40% forsterite/PLA hybrid nanocomposite scaffold group (G1) and the 70% forsterite/PLA hybrid nanocomposite scaffold group (G2), and the control group (G3) at two distinct time points of 4 and 8 weeks. Angiogenesis outcomes across the three groups were assessed using a one-way ANOVA. Post-hoc pairwise comparisons were conducted using Tukey's test. Furthermore, an independent samples t-test was utilized to compare osteogenic potential between the G1 and G2 scaffold groups, irrespective of the sacrifice time. Finally, tissue responses across the three experimental groups were statistically compared using the non-parametric Kruskal-Wallis test.

## RESULTS

Following the creation of 8mm diameter circular bone defects with a depth of 1.5mm in the parietal bone of the calvaria, the defects were implanted with forsterite/PLA hybrid nanocomposite scaffolds exhibiting varying porosities. Histological analysis conducted four weeks post-implantation revealed the development of both woven and lamellar bone. Furthermore, quantitative assessment at 8 weeks demonstrated the formation of a complete bone bridge in the G1 and G2 groups (Figures 2 and 3).

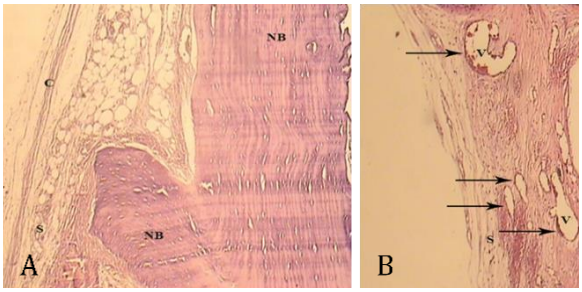


**Fig 2.** Forsterite/Poly Lactic Acid hybrid nanocomposite scaffold with 40% porosity (A) and with 70% porosity (B) in the calvari after 8 weeks (×100 magnification). S indicates the scaffold, NB indicates the newly formed bone, and C indicates the capsule. Complete bone bridging can be seen. Blood vessels with luminal structures containing red blood cells can be seen (arrow).

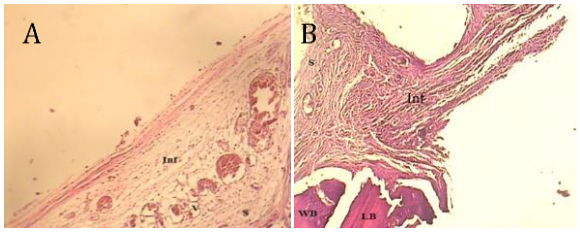


**Fig 3.** Forsterite/Poly Lactic Acid hybrid nanocomposite scaffold with 70% porosity (A) and 40% porosity (B) in the calvaria after 4 weeks (×100 magnification). S indicates the scaffold, V indicates blood vessels, LB indicates the lamellar bone, WB indicates the woven bone, and Inf indicates the inflammatory cells.

Table 1 delineates the mean percentages of bone formation and angiogenesis, alongside the temporal influence of the sacrifice time point on these parameters. Furthermore, it elucidates the interaction effect observed between the specific graft material employed and the designated sacrifice time. An ANOVA did not reveal any statistically significant differences in the investigated variables across the experimental groups. However, employing a two-way ANOVA, a statistically significant interaction effect between the graft material and the sacrifice time point on angiogenesis was identified (P=0.02). Consequently, a one-way ANOVA was subsequently applied for more detailed analysis (Table 1). Tukey's post hoc analysis indicated a statistically significant difference in angiogenesis within G1 at 4 and 8 weeks (P=0.03). Additionally, a statistically significant difference in the percentage of angiogenesis was observed between the two groups at 8 weeks (P=0.01). Table 2 summarizes the findings regarding tissue response across the three experimental groups. Based on the non-parametric Kruskal-Wallis test, no statistically significant differences in tissue response were detected among the three groups at either of the evaluated time points (P=0.67).

Statistical analysis employing a t-test to compare groups G1 and G2, irrespective of the sacrifice time point, revealed a substantial disparity in the mean percentage of lamellar bone formation (P=0.05). Furthermore, a statistically significant difference was observed between the two groups concerning the mean total bone percentage (P=0.05; Table 3).

**Table 1.** Mean percentage of bone formation and angiogenesis of 3 groups at 4 and 8 weeks

| | Time (week) | Group 1 (N=6) | Group 2 (N=6) | Control (N=6) | P[a] | P[b] | P[c] |
|---|---|---|---|---|---|---|---|
| **Percentage of woven bone formation** | 4 | 17.50±2.04 | 20.00±3.03 | 18.50±1.92 | 0.16 | 0.39 | 0.64 |
| | 8 | 18.75±1.21 | 19.50±1.92 | 19.00±1.61 | | | |
| **Percentage of lamellar bone formation** | 4 | 16.08±2.35 | 17.66±3.18 | 15.16±0.98 | 0.11 | 0.56 | 0.34 |
| | 8 | 15.41±1.20 | 17.66±2.67 | 16.16±2.29 | | | |
| **Total bone formation** | 4 | 33.58±4.32 | 33.76±6.20 | 33.66±2.29 | 0.11 | 0.42 | 0.53 |
| | 8 | 34.25±1.94 | 37.33±4.29 | 35.16±3.68 | | | |
| **Angiogenesis** | 4 | 4.58±1.04 | 4.83±1.63 | 5.33±1.83 | 0.07 | 0.12 | 0.02 |
| | 8 | 7.83± 264 | 4.16±1.29 | 5.41±1.59 | | | |

N: Number of rats in each time and group; Group 1: 40% porosity scaffold; Group 2: 70% porosity scaffold; [a] Group effect; [b] Time effect; [c] Interaction effect; P-values were calculated using two-way analysis of variance (ANOVA)

**Table 2.** Frequency, distribution, and mean tissue response levels across the groups at 4 and 8 weeks

| Group | G1[a] | G1[b] | G2[a] | G2[b] | Control[a] | Control[b] | P |
|---|---|---|---|---|---|---|---|
| **No inflammation (N)** | 2 | 0 | 1 | 1 | 2 | 2 | 0.67 |
| **Mild inflammation (N)** | 4 | 6 | 3 | 3 | 3 | 3 | |
| **Moderate inflammation (N)** | 0 | 0 | 2 | 1 | 1 | 1 | |
| **Severe inflammation (N)** | 0 | 0 | 0 | 1 | 0 | 0 | |
| **Mean inflammation level** | 1.66 | 2.00 | 2.16 | 2.33 | 1.83 | 1.83 | |

G1: Group 1 (40% porosity scaffold); G2: Group 2 (70% porosity scaffold); [a] At 4 weeks; [b] At 8 weeks; P-value was calculated using Kruskal Wallis test; Number of rats in each time and group was 6

**Table 3.** Percentage of woven, lamellar, and total bone formation in groups 1 and 2 irrespective of the sacrifice time

| Variable | N | Group | Mean ± SD | P |
|---|---|---|---|---|
| **Woven** | 12 | G1 | 18.12±1.73 | 0.07 |
| | | G2 | 19.75±2.43 | |
| **Lamellar** | 12 | G1 | 15.75±1.82 | 0.05 |
| | | G2 | 17.66±2.80 | |
| **Total bone** | 12 | G1 | 33.91±3.21 | 0.05 |
| | | G2 | 37.50±5.09 | |

N: number of rats in each group; G1: Group 1 (40% porosity scaffold); G2: Group 2 (70% porosity scaffold); P-value was calculated using a two tailed t-test.

## DISCUSSION

This study, evaluating the bone induction capacity of the scaffolds, demonstrated that in both groups, the newly generated bone tissue at the 4- and 8-week time points consisted of both lamellar and woven bones. While the mean percentage of bone development in G2 exhibited a marginal increase compared to the control group, both G2 and the control group displayed a greater percentage of new bone formation than G1. Nevertheless, these observed differences were not statistically significant.

In line with our findings, Weng et al. reported a significant difference in callus formation one month post-surgery between a control group and two groups treated with compact poly (l-lactic acid)/polycaprolactone (PLLA/PCL) macro-porous scaffolds. However, their study indicated that by two months, callus quantity was greater in both scaffold groups compared to the control (3), a result that our research did not corroborate.

Aligned with the findings of the present research, Rismanchian et al. observed no statistically significant variation in the mean percentage of woven bone between the control and forsterite scaffold groups at both 30- and 60-days post-implantation [20]. Conversely, within G1, a notable increase in the mean woven bone percentage was evident over the period from week 4 to week 8. This increase was likely attributed to the scaffold exhibiting a higher degree of degradation at this specific time point, which facilitated substantial bone tissue development. Generally, the rate of osteogenesis observed in G1 was lower compared to the other experimental groups. In G2, the mean percentage of woven bone at 8 weeks was less than that observed at 4 weeks, indicating an initially rapid pace of osteogenesis in this group that decreased quantitatively over the experimental period.

In a study by Montjovent et al., the deposition of lamellar bone was observed in several experimental groups, including PLLA/hydroxyapatite (HA), PLLA/β-tricalcium phosphate (T β-TCP), and β-TCP Mathys (Mathys, Bettlach, Switzerland). The control group also involved β-TCP Mathys. Their findings indicated that the rate of lamellar bone deposition was slower in the group treated with β-TCP Mathys compared to the other material combinations [21]. Their findings aligned with our observations, despite disparities in the methodological approaches and experimental designs of the two investigations. The mean percentage of lamellar bone in G2 was significantly higher compared to both G1 and the control group. Conversely, G1 exhibited a lower mean percentage of lamellar bone than the control group, suggesting a reduced rate of osteogenesis within this particular compact scaffold. Consistent with our current study, Rismanchian et al. reported no statistically significant difference in the mean lamellar bone percentage at day 30 between the control group and the forsterite scaffold group [20]. However, in contrast to our findings, their study indicated a significant divergence in the mean lamellar bone percentage between the forsterite and control groups. The observed disparity in outcomes may be attributed to variations in the type of scaffold employed, specifically the slow degradation rate inherent in the PLA scaffold. In G1, the mean percentage of lamellar bone at 8 weeks was lower compared to that at 4 weeks. Conversely, G2 and the control group exhibited a marginal increase in this parameter. A plausible interpretation for this phenomenon is that the formation of compact

lamellar bone necessitates a more protracted developmental period. Consequently, the quantity of lamellar bone formed at 4 weeks is comparatively less. Given the protracted osteogenic progression in G1, this condition was more pronounced within this cohort.

In G2, the mean percentage of total bone formation surpassed that of both the control group and G1, indicating a higher osteoconductive efficacy for the 70% porous scaffold. Conversely, G1 exhibited a lower bone formation rate compared to the control group. Thus, while the 40% porous scaffold demonstrated a reduced rate of osteogenesis, its structural integrity may be maintained for a longer duration in extensive bone defects. In contrast to our findings, Van der Pol et al. reported a higher rate of osteogenesis in the PLA/TCP biocomposite scaffold group compared to the negative control group after a 12-month period [5]. This discrepancy in results between the two studies may be attributed to variations in the experimental design and the duration of the observation period [5]. Within all experimental groups of the present study, the total quantity of bone formation exhibited a statistically insignificant increase between 4 and 8 weeks.

Based on the presented data, G1 and G2 exhibited complete bone bridge formation, seemed "biologically ideal," at the eight-week mark. This observation aligns with the findings reported by Montjovent et al. [21]. Furthermore, a statistically significant difference was noted in the mean percentage of lamellar bone between the two groups, with G2 demonstrating a higher percentage, irrespective of the specific time of sacrifice. This suggests a superior level of developed bone quality within the investigated group. Statistically significant differences in the mean total bone percentage between the two cohorts were observed, indicating enhanced osteoconductive properties in G2 compared to G1. These findings may be attributed to the presence of adequate interstitial space, facilitating optimal tissue ingrowth and the efficient diffusion of nutrients and metabolic byproducts. This observation diverged from the findings reported by Von Doernberg et al., whose study indicated an initial acceleration of scaffold degradation at the six-week mark, followed by a subsequent deceleration. Furthermore, their results suggested that the rate of bone formation did not keep pace with the rate of scaffold degradation [11].

The porous architecture of a scaffold is a critical factor influencing revascularization. However, the optimal pore size to facilitate this process and the biological implications of varying pore dimensions remain undetermined. In this study, a statistically significant difference in the mean percentage of vascularization was observed in G1 between 4 and 8 weeks. This suggests that angiogenesis was less pronounced in G1 at 4 weeks but increased by 8 weeks. This temporal change may be attributed to scaffold degradation and subsequent blood vessel ingrowth, or potentially to inflammatory responses within the material. At the fourth week of the study, the rate of angiogenesis in G1 was observed to be lower in comparison to the other two experimental groups. This is likely attributable to the dense microstructure of the scaffold material in G1, which impeded the ingrowth of blood vessels into the matrix. Conversely, G2, characterized by a high degree of porosity, exhibited a more pronounced initial vascular penetration. This process of vascularization, progressed without apparent hindrance throughout the duration of the observation period. The mean percentage of angiogenesis observed in G1 at 8 weeks exhibited a marginal increase compared to the control group; however, this difference was not statistically significant, potentially attributable to the presence of inflammation. Similarly, the research conducted by Rossiet et al. indicated a disparity in the rate of vascularization and the depth of penetration into scaffolds characterized by varying degrees of porosity. Furthermore, their findings revealed that scaffolds with higher porosity exhibited larger vessel diameters [22]. This scaffold, lacking cells and growth factors, relied solely on the in situ hematoma and blood clot for cellular stimulation. Consequently, the data suggest that the scaffold provided adequate support for the

clot without eliciting any detrimental effects. In the current research, the extent of inflammatory responses did not significantly differ between G1 and G2. This research aligns with the findings reported by von Dornberg et al. [11]. During the initial phases of tissue repair, neutrophils are the predominant immune cells, drawn to the injury site by chemokines released from damaged cells. After that, monocytes, macrophages, and fibroblasts become the dominant cell types, leading to the formation of dense fibrous tissue primarily composed of fibroblasts and a collagen matrix. Weng et al. documented the presence of neutrophils and fibroblasts solely within compact PLLA and PLLA/PCL macro-pore scaffolds, while these cells were not observed in the control group [3].

The forsterite/PLA hybrid nanocomposite scaffold exhibited minimal adverse effects on the healing process in our observations, indicating its low cytotoxicity and biocompatibility. Its tolerability within the human body, without eliciting significant adverse reactions, suggests a positive impact on bone tissue engineering applications. Consequently, this scaffold demonstrates potential utility in bone tissue engineering, particularly with the possibility of surface modification using cells and/or growth factors.

## CONCLUSION

The present study demonstrated the potential of a forsterite-PLA hybrid nanocomposite scaffold for clinical application in enhancing bone regeneration. Histological analysis at 4 and 8 weeks revealed the formation of both woven and lamellar bone within the scaffold groups exhibiting 40% and 70% porosity. The scaffold exhibiting 70% porosity demonstrated superior efficacy in promoting osteogenesis, both qualitatively and quantitatively. Conversely, complete bone bridging was observed in both experimental groups after 8 weeks. Limited and controlled inflammatory responses were noted in both cohorts. Consequently, forsterite/PLA scaffolds fabricated via fused deposition modeling hold promise for enhancing the regeneration of substantial bone defects due to their adequate mechanical stability.

## ACKNOWLEDGEMENT

The authors would like to thank the Vice-chancellor for Research and Technology at Isfahan University of Medical Sciences for providing support for this work.

## CONFLICT OF INTEREST STATEMENT

None declared.

## REFERENCES

1. Pelegrine, A. A.; Da Costa, C. E. S.; Sendyk, W. R.; Gromatzky, A., The comparative analysis of homologous fresh frozen bone and autogenous bone graft, associated or not with autogenous bone marrow, in rabbit calvaria: a clinical and histomorphometric study. Cell and tissue banking 2011, 12, (3), 171-184.
2. Elgendy, E. A.; Shoukheba, M. Y. M., Histological and Histomorphometric Study of the Effect of Strontium Ranelate on the Healing of One-Wall Intrabony Periodontal Defects in Dogs. Journal of Cytology & Histology 2012, 3, 3-6.
3. Weng, W.; Song, S.; Cao, L.; Chen, X.; Cai, Y.; Li, H.; Zhou, Q.; Zhang, J.; Su, J., A comparative study of bioartificial bone tissue poly-l-lactic acid/polycaprolactone and PLLA scaffolds applied in bone regeneration. Journal of Nanomaterials 2014, 2014.
4. Ibim, S. E.; Uhrich, K. E.; Attawia, M.; Shastri, V. R.; El-Amin, S. F.; Bronson, R.; Langer, R.; Laurencin, C. T., Preliminary in vivo report on the osteocompatibility of poly (anhydride-co-imides) evaluated in a tibial model. Journal of biomedical materials research 1998, 43, (4), 374-379.
5. van der Pol, U.; Mathieu, L.; Zeiter, S.; Bourban, P.-E.; Zambelli, P.-Y.; Pearce, S. G.; Bouré, L.; Pioletti, D. P., Augmentation of bone defect healing using a new biocomposite scaffold: an in vivo study in sheep. Acta Biomaterialia 2010, 6, (9), 3755-3762.
6. Ge, Z.; Tian, X.; Heng, B. C.; Fan, V.; Yeo, J. F.; Cao, T., Histological evaluation of osteogenesis of 3D-printed poly-lactic-co-glycolic acid (PLGA) scaffolds in a rabbit model. Biomedical materials 2009, 4, (2), 021001.
7. Kharaziha, M.; Fathi, M., Improvement of mechanical properties and biocompatibility of forsterite bioceramic addressed to bone tissue engineering materials. Journal of the mechanical behavior of biomedical materials 2010, 3, (7), 530-537.
8. Xiao, X.; Wang, W.; Liu, D.; Zhang, H.; Gao, P.; Geng, L.; Yuan, Y.; Lu, J.; Wang, Z., The promotion of

angiogenesis induced by three-dimensional porous beta-tricalcium phosphate scaffold with different interconnection sizes via activation of PI3K/Akt pathways. Scientific reports 2015, 5, (1), 1-11.
9. Karande, T. S.; Ong, J. L.; Agrawal, C. M., Diffusion in musculoskeletal tissue engineering scaffolds: design issues related to porosity, permeability, architecture, and nutrient mixing. Annals of biomedical engineering 2004, 32, (12), 1728-1743.
10. Goldstein, A. S.; Zhu, G.; Morris, G. E.; Meszlenyi, R. K.; Mikos, A. G., Effect of osteoblastic culture conditions on the structure of poly (DL-lactic-co-glycolic acid) foam scaffolds. Tissue engineering 1999, 5, (5), 421-433.
11. von Doernberg, M.-C.; von Rechenberg, B.; Bohner, M.; Grünenfelder, S.; van Lenthe, G. H.; Müller, R.; Gasser, B.; Mathys, R.; Baroud, G.; Auer, J., In vivo behavior of calcium phosphate scaffolds with four different pore sizes. Biomaterials 2006, 27, (30), 5186-5198.
12. Wang, B. Y.; Fu, S. Z.; Ni, P. Y.; Peng, J. R.; Zheng, L.; Luo, F.; Liu, H.; Qian, Z. Y., Electrospun polylactide/poly (ethylene glycol) hybrid fibrous scaffolds for tissue engineering. Journal of Biomedical Materials Research Part A 2012, 100, (2), 441-449.
13. Hoque, M. E., Advanced applications of rapid prototyping technology in modern engineering. BoD–Books on Demand: 2011.
14. Naghieh, S.; Foroozmehr, E.; Badrossamay, M.; Kharaziha, M., Combinational processing of 3D printing and electrospinning of hierarchical poly (lactic acid)/gelatin-forsterite scaffolds as a biocomposite: Mechanical and biological assessment. Materials & Design 2017, 133, 128-135.
15. Naghieh, S.; Badrossamay, M.; Foroozmehr, E.; Kharaziha, M., Combination of PLA micro-fibers and PCL-gelatin nano-fibers for development of bone tissue engineering scaffolds. Int. J. Swarm Intell. Evol. Comput 2017, 6, (1), 1-4.
16. Aeinehchi, M.; Eslami, B.; Ghanbariha, M.; Saffar, A., Mineral trioxide aggregate (MTA) and calcium hydroxide as pulp-capping agents in human teeth: a preliminary report. International endodontic journal 2003, 36, (3), 225-231.
17. Ooms, E.; Egglezos, E.; Wolke, J.; Jansen, J., Soft-tissue response to injectable calcium phosphate cements. Biomaterials 2003, 24, (5), 749-757.
18. Cintra, L. T. A.; Bernabé, P. F. E.; Moraes, I. G. d.; Gomes-Filho, J. E.; Okamoto, T.; Consolaro, A.; Pinheiro, T. N., Evaluation of subcutaneous and alveolar implantation surgical sites in the study of the biological properties of root-end filling endodontic materials. Journal of Applied Oral Science 2010, 18, 75-82.
19. Jabbarzadeh, E.; Starnes, T.; Khan, Y. M.; Jiang, T.; Wirtel, A. J.; Deng, M.; Lv, Q.; Nair, L. S.; Doty, S. B.; Laurencin, C. T., Induction of angiogenesis in tissue-engineered scaffolds designed for bone repair: a combined gene therapy–cell transplantation approach. Proceedings of the National Academy of Sciences 2008, 105, (32), 11099-11104.
20. Rismanchian, M.; Nosouhian, S.; Razavi, S. M.; Davoudi, A.; Sadeghiyan, H., Comparing three different three-dimensional scaffolds for bone tissue engineering: an in vivo study. The journal of contemporary dental practice 2015, 16, (1), 25-30.
21. Montjovent, M. O.; Mathieu, L.; Schmoekel, H.; Mark, S.; Bourban, P. E.; Zambelli, P. Y.; Laurent-Applegate, L. A.; Pioletti, D. P., Repair of critical size defects in the rat cranium using ceramic-reinforced PLA scaffolds obtained by supercritical gas foaming. Journal of Biomedical Materials Research Part A: An Official Journal of The Society for Biomaterials, The Japanese Society for Biomaterials, and The Australian Society for Biomaterials and the Korean Society for Biomaterials 2007, 83, (1), 41-51.
22. Rossi, L.; Attanasio, C.; Vilardi, E.; De Gregorio, M.; Netti, P., Vasculogenic potential evaluation of bottom-up, PCL scaffolds guiding early angiogenesis in tissue regeneration. Journal of Materials Science: Materials in Medicine 2016, 27, (6), 107.